



ORIGINAL ARTICLE

Ionic liquid assisted growth of poly(3,4-ethylenedioxythiophene)/reduced graphene oxide based electrode: An improved electro-catalytic performance for the detection of organophosphorus pesticides in beverages



Shweta Rana ^{a,*}, Ranjeet Kaur ^a, Roshni Jain ^a, Nirmal Prabhakar ^b

^a Department of Chemistry, Panjab University Chandigarh, 160014, India

^b Department of Biochemistry, Panjab University Chandigarh, 160014, India

Received 6 June 2018; accepted 19 August 2018

Available online 27 August 2018

KEYWORDS

PEDOT/ILRGO electrodes;
Impedimetry;
Electrocatalysis;
Voltammetry;
Pesticides

Abstract An enzyme based nanocomposite host matrix comprising of Poly(3,4-ethylenedioxythiophene) and 1-Butyl-3-methylimidazolium trifluoromethanesulfonate based ionic liquid functionalized reduced graphene oxide (PEDOT/ILRGO) has been designed for the electrochemical detection of organophosphorus pesticides (OPs). Interactions between reduced graphene oxide and ionic liquid have resulted in better loading of the same onto the PEDOT matrix. A detail redox analysis highlights the increased surface area and more number of charge carriers enabling the redox inhibition mechanism more efficient in the designed electrode. The biosensor works on the principle of generation of thiocholine by reaction between acetylcholinesterase (AChE) and substrate acetylthiocholine iodide (ATChI), which undergoes oxidation resulting in redox peaks. Under the optimized conditions, three different OPs chlorpyrifos (CP), malathion (ML) and methyl parathion (MP) were analyzed by varying concentrations with limit of detection calculated to be 0.04 ng ml⁻¹, 0.117 ng ml⁻¹ and 0.108 ng ml⁻¹ respectively, all below 0.2 μg ml⁻¹ concentration which is their maximum residual limit, hence exhibiting good sensitivity. The prepared sensor offers 91.7% of reactivation and good stability for 15–20 days with 95.7% of initial current response retainment, reflecting its excellent potency as an organophosphorus pesticide sensor.

© 2018 Production and hosting by Elsevier B.V. on behalf of King Saud University. This is an open access article under the CC BY-NC-ND license (<http://creativecommons.org/licenses/by-nc-nd/4.0/>).

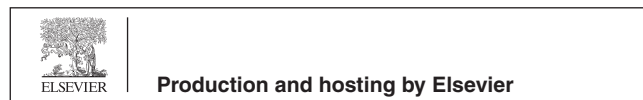
* Corresponding author.

E-mail address: shweta0402@pu.ac.in (S. Rana).

Peer review under responsibility of King Saud University.

1. Introduction

Since the last few decades, organophosphorus pesticides (OPs) have been widely used in agriculture to exterminate pest-borne diseases due to their easy availability and low cost. But,



unfortunately the cases of their hazardous effects outnumber the advantages they offer to the mankind (Kumar et al., 2015). The health alarms of OPs include fatigue, headache, dizziness, inability to walk and simultaneously make human body susceptible to diseases such as cancer, reproductive and neurological disorders. Hence considering these, there is a dire need for their detection even at trace levels (Chowdhary et al., 2014). The contemporary methods for pesticide detection include solid phase extraction (Liu et al., 2018), chromatography (Huang et al., 2018a,b,c), spectrophotometric methods (Harshit et al., 2017) and fluorimetric methods (Obare et al., 2010). But these techniques require expensive and sophisticated instrumentation as well as conscientious and labor intensive sample preparations (Chowdhary et al., 2014; Bhadekar et al., 2011).

Recently, enzyme linked immunosorbents have also been developed for the detection of various pesticides at trace levels with good reactivation. But, time requirements and series of steps limit their applications (Yao et al., 2017; Liu et al., 2017; Xie et al., 2017). Recently, various photoelectrochemical and amperometric biosensors have also been deployed for sensing different analytes. But despite some advances in this field they are limited to steric hinderance effect, electron acceptor/donor production and energy transfer effect (Shu et al., 2018; Qiu et al., 2018; Lv et al., 2018; Shu and Tang, 2017; Tang et al., 2006). In this regard, electrochemical biosensors being single step and fast field assay have ability to compliment the analytical methods by eliminating tedious preparation with highly developed instrumentation and hence making field testing easier and faster with significant decrease in cost per analysis (Pundir and Chauhan, 2012; Farghaly et al., 2014). The most commonly reported electrochemical biosensors deployed for the detection of OPs involve enzyme acetylcholinesterase (AChE), which is inhibited due to toxicity of OPs (Liu et al., 2015). Hence, this mechanism can be easily utilized for the perceptible change in the electrochemical signal in the designed biosensor.

For designing an efficient biosensor, enzyme immobilization is an important key factor and for this higher surface area and faster charge transfer rate are few major factors that are required to be considered for a better catalytic activity while selecting the electrode material (Kumar et al., 2015). Literature is full of such materials where catalytic activity has been enhanced by introducing novel structures (Huang et al., 2018a,b,c, 2014). In particular to enzyme catalysis, conducting polymers have attracted remarkable attention as efficient immobilizing matrices for biomolecules owing to their high currents and faster electron transfer rate that can be easily enforced by exploiting their attribute of structural flexibility (Moyo et al., 2012). Amongst various conducting polymers poly(3,4-ethylenedioxythiophene) (PEDOT) is one of the exciting candidate due to its excellent biocompatibility, low redox potential and high conductivity (Sikora et al., 2011; Bhandari et al., 2009) but its poor solubility and weak mechanical strength limits its use as electrode material. To overcome these effects the surface of PEDOT can be immobilized with carbon nanomaterials which provides enhanced mechanical strength, large surface area and improved conductivity favorable for its use as efficient electrode material (Shen et al., 2013; Saxena et al., 2010). Wei et al. have utilized the porosity of these carbon based materials for efficient AChE immobilization thereby boosting the biosensor performance for the detec-

tion of OPs (Wei and Wang, 2015). Along with porosity, carbon structure used by them had provided high stability, ionic conductivity and wide electrochemical window which ultimately enhance the response sensitivity and facilitate faster electron transfer rate. In literature, particularly graphene based carbon structures and their composites have consistently found to give remarkably high efficiency results for the pesticide detection (Bahadır and Sezgintürk, 2016). Wang et al. have used carboxylic graphene decorated with ZnO nanoparticles for enzymatic detection of pesticides where the synergistic integration of these nanostructures has remarkably increased the sensitivity and limit of detection of the biosensor (Wang et al., 2014).

The gripping of reduced graphene oxide is relatively low directly onto the surface of PEDOT which in turn reduces the redox active sites present in the system. To bridge the gap between the two, ionic liquids can be used which endow the dissemination of larger surface area and better redox activity to the electrode material. The ionic liquids not only provides the heterogeneous nature to the electrode but also makes it easy as pie to develop novel composite to use as electrode material for organophosphorus pesticides sensing (Shen et al., 2013; Saxena et al., 2010). Zheng et al. have incorporated faster electron transfer rate attribute in graphene using ionic liquid and gelatin as an efficient matrix for AChE adhesion thereby making a low cost, high sensitivity sensor (Zheng et al., 2015).

Hence, after analyzing the unique features of PEDOT and carbon based nanostructures from literature herein, we have designed an electroactive matrix of PEDOT-reduced graphene oxide functionalized by ionic liquid (PEDOT/ILRGO) for effective immobilization of acetylcholinesterase enzyme (Wu et al., 2015; Huang et al., 2015). In our case, imidazolium ring of the chosen ionic liquid prevents the stacking between the layers of reduced graphene oxide and hence increases the wettability of the surface. Though, composites of conducting polymers with reduced graphene oxide have been utilized in the literature for other sensing applications (Taylor et al., 2017; Sundramoorthy et al., 2016) but till now they have not been used for the detection of OPs and in particular for the simultaneous determination of three most hazardous pesticides, this is the first report to best of our knowledge. Moreover, here the ability of electrodes are further augmented by use of ionic liquid as a novel approach yielding a better electrochemical sensor for organophosphorus pesticides as confirmed in its detailed comparative redox analysis.

2. Experimental

2.1. Reagents

Chlorpyrifosmethyl, malathion, methyl parathion, acetylthiocholine Iodide (ATChI), AChE (1000 Units/mg, from electric eel) and 2-pyridinealdehyde methiodide (2-PAM) were purchased from Sigma-Aldrich. 3,4-Ethylenedioxythiophene (EDOT) and graphite were also obtained from Sigma-Aldrich. Phosphate buffer solutions (PBS) were prepared using di-sodium hydrogen orthophosphate anhydrous from Fluka and sodium dihydrogen phosphate monohydrate from Fischer scientific. 1S-(+)-10-camphorsulfonic acid (CSA), lithium trifluoromethanesulfonate (98%) and hydrazine monohydrate

(64%) were obtained from Acros organics whereas, ionic liquid 1-Butyl-3-methylimidazolium trifluoromethanesulfonate was procured from Merck (Germany). Inorganic transparent electrodes of fluorine doped tin oxide (FTO) coated glass electrodes were obtained from Sigma-Aldrich and were cleaned in a soap solution, 30% HCl solution, double distilled water and acetone prior to use. All the interference studies were done using following ions: [cadmium chloride, ascorbic acid, dopamine (Hi-Media), urea (British drug house), citric acid (Merck), cupric sulphate (Qualigens) and nickel chloride (central drug house)]. Deionized water was obtained from mili-Q-system.

2.2. Instrumentation

The FTIR analysis for electrode characterization was recorded on Nicolet IS50 FTIR spectrophotometer. X-ray diffraction (XRD) patterns were collected using X-ray diffractometer (spinner3064XPRT-PRO) using $\text{CuK}\alpha$ radiation operating in the 2θ range from 0° to 80° . The surface of films was investigated using Field Emission Scanning Electron Microscope (FE-SEM -SU8010-Hitachi) and the contact angle studies were performed using Model DSA100 with the help of sessile drop method. Electrochemical response was confirmed using Autolab cyclic voltammeter hooked with research electrochemical software and equipped with three electrode electrochemical cell consisting of Ag/AgCl/KCl as reference, a film on fluorine doped tin oxide coated glass as working electrode and Pt was used as counter electrode.

2.3. Fabrication of biosensing electrode

2.3.1. Synthesis of reduced graphene oxide (RGO)

To 2 g of graphite powder H_2SO_4 and HNO_3 in 3:1 volume ratio was added. The mixture was then refluxed at 40°C for 16 h. The resulting mixture was then ultrasonicated, centrifuged and washed with deionized water to attain pH value within 5–6 range and then air dried at 60°C . The dispersion of product was then prepared by using 0.07 wt% of graphite oxide (GO) in deionized water and subjected to ultrasonication. To 40 ml of this dispersion, 24 μL of hydrazine and 180 μL of 25% ammonia solution were added and refluxed at $90\text{--}95^\circ\text{C}$ for 1 h. The solution was then centrifuged, precipitated and air dried at 60°C .

2.3.2. Synthesis of ionic liquid functionalized reduced graphene oxide (ILRGO)

The dispersion of graphite oxide was prepared by using 0.07 wt% of graphite oxide (GO) in deionized water and was processed to ultrasonication for about an hour. The resulting solution was then mixed with 200 μL ionic liquid to obtain a colloidal suspension. The mixture was subjected to reflux at $90\text{--}100^\circ\text{C}$ with addition of 24 μL of hydrazine and 180 μL of 25% ammonia solution to obtain ionic liquid functionalized reduced graphene oxide.

2.3.3. Preparation of neat PEDOT electrodes

For fabrication of neat PEDOT films, solution of 0.1 M 3,4-ethylenedioxythiophene (EDOT), 1 M camphorsulphonic acid and 0.1 M lithium trifluoromethanesulfonate was prepared in

deionized water. Electrodeposition of films were done using three electrode cell at constant potential of +1.2 V where Pt acts as auxiliary electrode, Ag/AgCl as reference electrode and $\text{SnO}_2\text{:F}$ glass electrode as working electrode. The resulting blue colored films of PEDOT were immediately rinsed with water, acetone and dried in air prior to use.

2.3.4. Preparation of modified PEDOT/ILRGO electrode

A colloidal dispersion of monomer solution of EDOT with ionic liquid functionalized reduced graphene oxide added in 25 ml of deionized water was used for the preparation of PEDOT/RGO/IL films at constant potential of +1.2 V for 100 s. The dispersion was ultrasonicated prior to use.

2.3.5. Preparation of biosensors

For the fabrication of biosensor, 5 μL of enzyme was immobilized onto PEDOT/ILRGO films by drop casting method. The films were kept at 4°C for 24 h for maximum physical adsorption and then soaked in 0.1 M buffer in order to remove loosely bound enzyme (Fig. 1). These biosensor films were preserved at 4°C to maintain enzymatic activity when not in use.

3. Results and discussion

3.1. FTIR and XRD studies

FTIR spectra of GO, RGO and ILRGO (Fig. S1) are in good agreement with already reported work. In case of GO a broad hump between 3000 and 3500 cm^{-1} is due to —OH group and a peak at 1624 cm^{-1} is due to —OH bending vibrations of absorbed water molecules causing hydrophilic nature of GO (Shahriary and Athawale, 2014). The stretching vibrations due to C=O stretching of carboxylic acid group are present at 1710 cm^{-1} (Soltani and Lee, 2017). The oxygen functionalities in RGO are comparatively lesser as indicated by the lower peak intensities. Also a peak between 1350 and 1600 cm^{-1} observed in the case of RGO, is indicative of skeletal vibrations of sheet like structure of graphene (Wu et al., 2012; Ji et al., 2012). FTIR spectra of both RGO and ILRGO exhibits the characteristic peaks of —C=C— bonds at 1620 cm^{-1} . Generally, covalent interactions perturbs the —C=C— structure of RGO due to conversion of sp^2 to sp^3 hybridized carbon atoms, resulting in decrease of intensity of peaks. But, Fig. S1 clearly shows that after functionalization of surface of RGO with ionic liquids, the peaks intensities of —C=C— increases pointing towards $\langle\text{pi-pi}\rangle$ interactions between the molecules (Karthik et al., 2018).

The successful fabrication of GO, RGO and ILRGO were also confirmed by X-ray diffraction (XRD) as shown in Fig. 2. The diffraction peak (0 0 1) in case of GO appears at 9.24° with inter-planar spacing of 0.96 nm. This indicates the successful functionalization of graphite with oxygen functionalities (Soltani and Lee, 2017). The appearance of small intensity diffraction peak (0 0 2) at $2\theta = 15^\circ$ indicates the presence of partially reduced graphene oxide (prGO) in small amount (Lee et al., 2015). Appearance of broad peak in RGO, from $2\theta = 20^\circ$ to 30° (d-spacing = 0.37 nm) is attributed to revitalization of vanderwaal's interaction upon reduction of graphene oxide (Muthoosamy et al., 2015). The broadness in

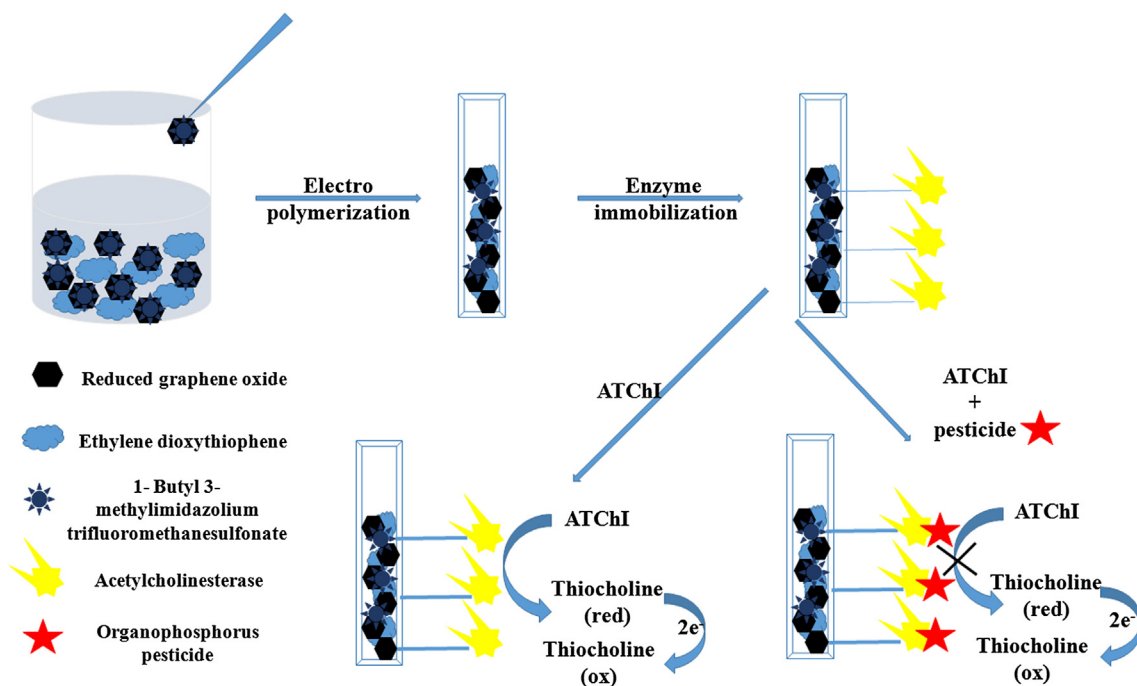


Fig. 1 Schematic diagram showing fabrication of PEDOT/ILRGO/AChE based biosensor and its behavior towards organophosphorus pesticides.

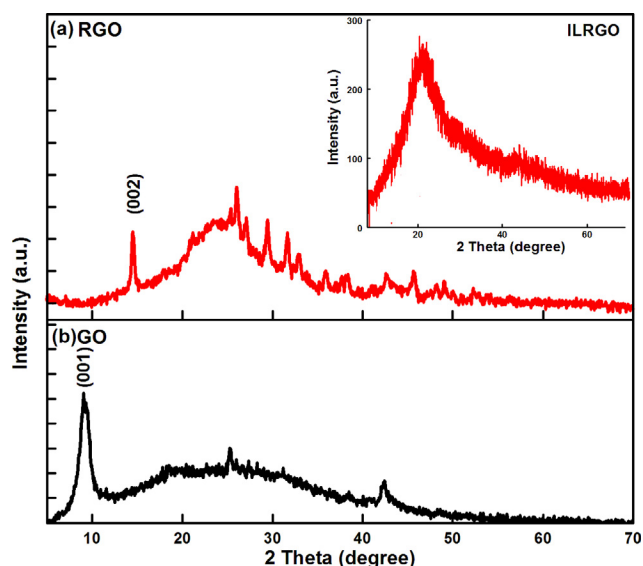


Fig. 2 X-ray diffraction patterns of (a) reduced graphene oxide (RGO), inset showing the XRD of ILRGO and (b) graphene oxide (GO).

peak indicates the loss of long range order in the graphene sheets as they are stacked with few-layers (De Silva et al., 2012). In addition, the loss of oxygenous groups and water molecules occur from the surface of graphene oxide as indicated by decreased interlayer spacing. In case of ILRGO, the peak shifts to $2\theta = 21^\circ$, which indicates the increased interplanar spacing due to ionic liquid functionalization of RGO.

3.2. FESEM studies

Surface morphology of the films was investigated using FESEM. Fig. 3(b) shows the flaked structure of ILRGO where discrete exfoliated graphene sheets are clearly ostensible. The dimensions of the sheets range from few nanometers to several micrometers as clearly gauged from the FESEM image. Absence of functional groups in the RGO (Fig. 3(a)) prevents stacking in between the graphene sheets resulting in ripple like effect in surface morphology. The colloidal dispersion containing reduced graphene oxide and ionic liquid results in exfoliation of sheets of reduced graphene oxide and prevents its stacking. This is due to non-covalent or π - π interactions (as already described in FTIR) taking place between the molecules in the solution as shown in Fig. 4.

In FESEM image of PEDOT/ILRGO film, (Fig. 3(c)) homogeneous globular morphology and highly porous surface structure in the matrix is distinctly visible. It can be seen from Fig. 3(c, d) that scale like ILRGO are stacked on PEDOT matrix which is helpful in increasing the effective surface area, one of the essential prerequisite of the efficient bioelectrode. At higher magnification, (Fig. 3d) this flaked like structure of ILRGO is perceptible. As RGO stacking onto to PEDOT matrix is relatively low, it is augmented by the use of ionic liquid as shown in Fig. 3(c, d). The functionalization of surface of RGO with IL results in increased hydrophilicity which inturn increases the loading of enzyme onto its surface. This can be inferred from contact angle measurements as shown in Fig. S2. The contact angle in case of RGO is 30° whereas it decreases to 23.8° in case of ILRGO, due to increase hydrophilicity facilitated by ionic liquid. Thus changing nature of surface affects its surface properties and hence affects its activity. These type of structures helps in immobilization of

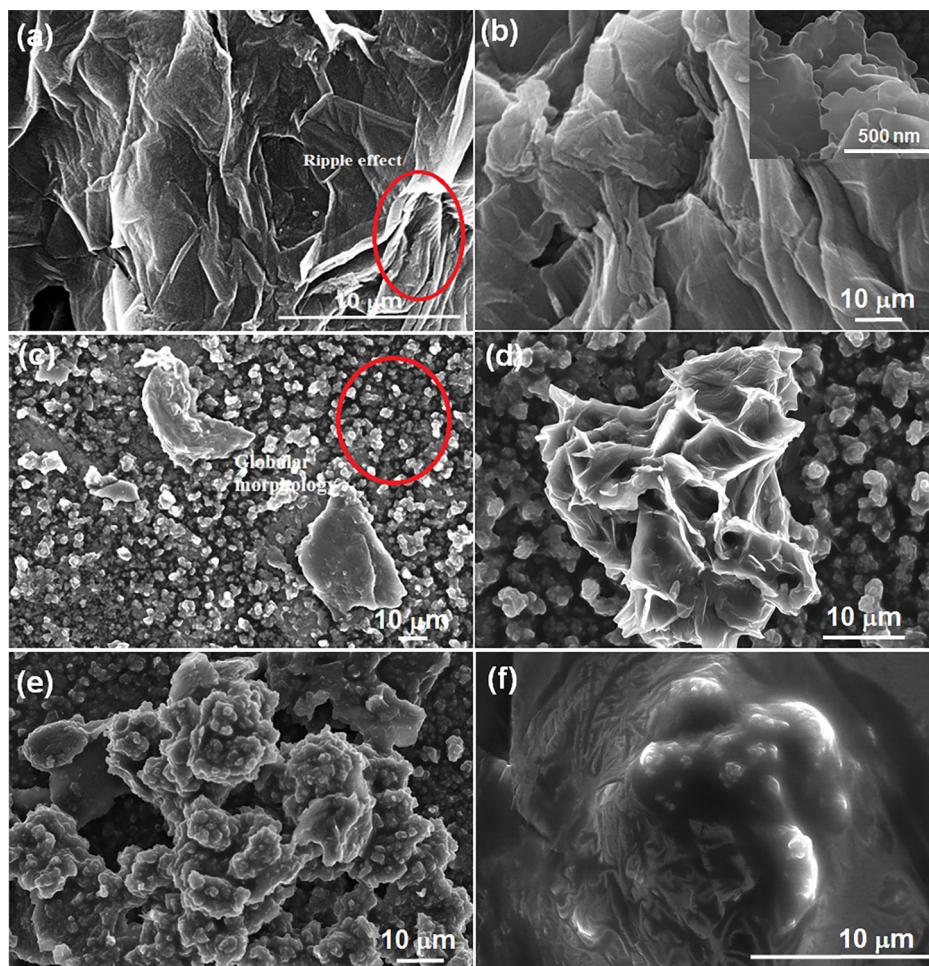


Fig. 3 FE-SEM images of (a) RGO, (b) ILRGO, (c) PEDOT/ILRGO, at low magnification and (d) at higher magnification, (e) PEDOT/ILRGO-AChE, at lower and (f) higher magnification.

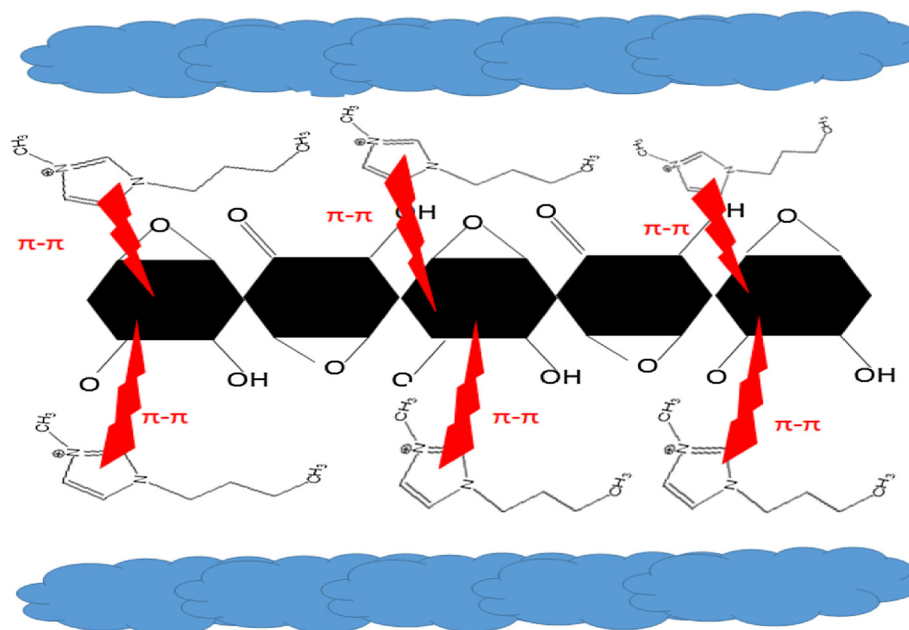


Fig. 4 Schematic diagram showing the interactions present between the molecules of reduced graphene oxide and ionic liquid.

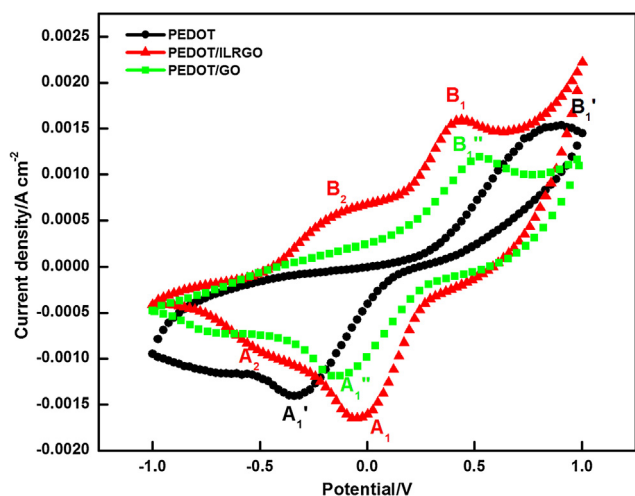
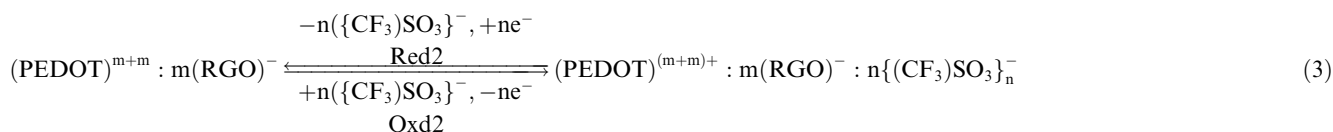
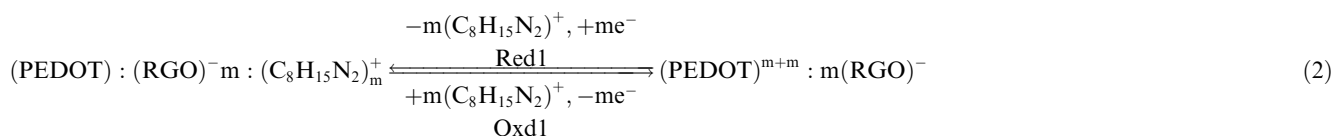
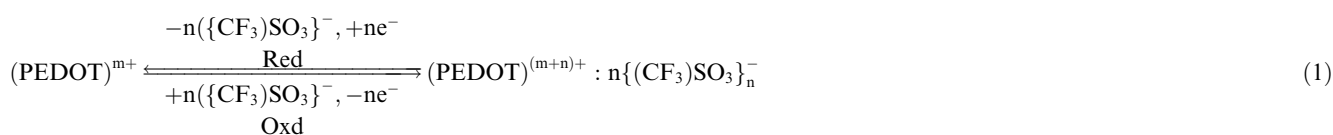


Fig. 5 Cyclic voltammograms of (●) neat PEDOT, (▲) PEDOT/ILRGO (■) PEDOT/GO in phosphate buffer (0.1 M, pH 7.4), having 5 mM $[\text{Fe}(\text{CN})_6]^{-3/-4}$ in 0.1 M KCl as a redox probe at 75 mV/s.

large amounts of enzyme on electrode due to increased surface area as shown in Fig. 3(e, f).



3.3. Electrochemical studies

In order to probe the change in electrochemical attributes of PEDOT/ILRGO, it was electrochemically analyzed in comparison with neat PEDOT film using cyclic voltammetry (CV) (scan rate of 75 mV/s) in a phosphate buffer (PBS pH 7.4) containing 5 mM $[\text{Fe}(\text{CN})_6]^{-3/4}$ and 0.1 M KCl as redox probes (25 °C) (Fig. 5). In neat PEDOT film cathodic peak (A_1') appears at -0.35 V and an anodic hump (B_1') at $+0.87$ V due to anion migration during the process whereas, the redox phenomenon occurring at PEDOT/ILRGO is completely different. The cathodic peak (A_1) at $+0.43$ V and anodic peak (B_1) at -0.05 V is attributed to anions migration as seen in neat PEDOT. The hump (B_2) at -0.046 V which is attributed to cation extraction accompanied by the ionic liquid hinting at

bipolaron formation, is completely absent in the neat PEDOT film. Well resolved peaks with higher current values and larger area under curve clearly show that not only the capacitive character has increased but electrochemical activity of films has also increased due to incorporation of ionic liquid functionalized reduced graphene oxide in PEDOT matrix. This is attributed to the enhanced conductivity provided by the regain of sp^2 hybridized lattice of reduced graphene oxide adding to better electrocatalytic performance.

On comparing the voltammogramic response of PEDOT/ILRGO with PEDOT/GO a decrease in current response was observed mainly because of lower conductivity, and repulsions between the two surfaces leading to less incorporation of its sheets onto the polymer matrix. When we load ILRGO onto PEDOT layers, the peak current gets enhanced due to regain of sp^2 hybridized structure and lesser repulsions between the two. The redox peaks in PEDOT/GO have lesser area, pointing towards hindrance in electron transfer between the analyte and underlying electrode in comparison to PEDOT/ILRGO. This higher electrochemical performance in PEDOT/ILRGO is due to ILRGO which endows the dissemination of larger surface area and better redox activity of electrode material due to less stacking efficiency in comparison to GO. The redox phenomenon occurring in the above electrodes are shown in the equations below.

Further, dependence of oxidation-reduction phenomena of the electrodes on scan rates are shown in Fig. S3. A linear relationship between the peak currents with square root of scan rate was obtained suggesting the presence of surface confined redox active sites in both the films. The diffusion coefficient values based on Randles-Sevcik equation (Narayana et al., 2014) are 5.62×10^{-15} cm^2/sec and 3.2×10^{-14} cm^2/sec for neat PEDOT and PEDOT/ILRGO respectively. These values clearly indicate diffusion controlled charge transfer phenomenon which is faster in case of PEDOT/ILRGO due to enhanced redox active surface area and porous nature of reduced graphene oxide. The faster charge transfer rate in PEDOT/ILRGO is attributed to the more effective counter ions provided by the imidazolium based ionic liquid. This also directs towards higher conductivity of reduced graphene and greater number of ions furnished by ionic

liquid enabling better electric linkage of electrode with increased number of redox active sites. This was further supported with the help of surface concentration calculation using equation (Fragkou et al., 2012):

$$I_p = n^2 F^2 A \Gamma v / 4RT \quad (4)$$

where n is number of electrons transferred, F is faraday constant, Γ is surface concentration (mol cm^{-2}) of neat PEDOT and PEDOT/ILRGO, A is surface area of electrode, v is scan rate (V/s) and I_p is peak current (A). The value of surface concentration of PEDOT/ILRGO ($19.07 \times 10^{-6} \text{ mol cm}^{-2}$) is higher in comparison of neat PEDOT ($7.92 \times 10^{-6} \text{ mol cm}^{-2}$) which is again attributed to loading of ILRGO as indicated in FESEM images (Fig. 3) and contributes towards the enhanced current response.

The electroactive surface area of neat PEDOT and PEDOT/ILRGO modified electrodes were calculated using chronocoulometry using Anson equation (Ahmed and Reifsnider, 2011) (Fig. S4) i.e.

$$Q = 2nFACD^{1/2}\pi^{1/2}t^{1/2} \quad (5)$$

where, Q represents the charge in Coulombs, n and A represents the number of electrons involved in electrochemical process and electrochemical active surface area of working electrode (cm^2), C represents the concentration of mediator (5 mM or $5 \times 10^{-6} \text{ mol/cm}^3$) and D and t represents diffusion coefficient of mediator and time of the system. The calculated electrochemical active surface area for neat PEDOT and PEDOT/ILRGO films are 0.131 cm^2 and 0.161 cm^2 respectively which again hints at better redox activity of latter enabling it as a better matrix for enzyme immobilization.

In order to calculate the interfacial charge transfer properties and to study the redox behavior, electrochemical impedance spectroscopic (EIS) analysis was done within the frequency range $0.1\text{--}10^5 \text{ Hz}$. Fig. 6(a) shows the Nyquist plots of neat PEDOT and PEDOT/ILRGO modified electrodes within specified frequency range. In lower frequency region the diffusion process dominates over the impedance phenomenon as it is the slowest event. Towards the higher

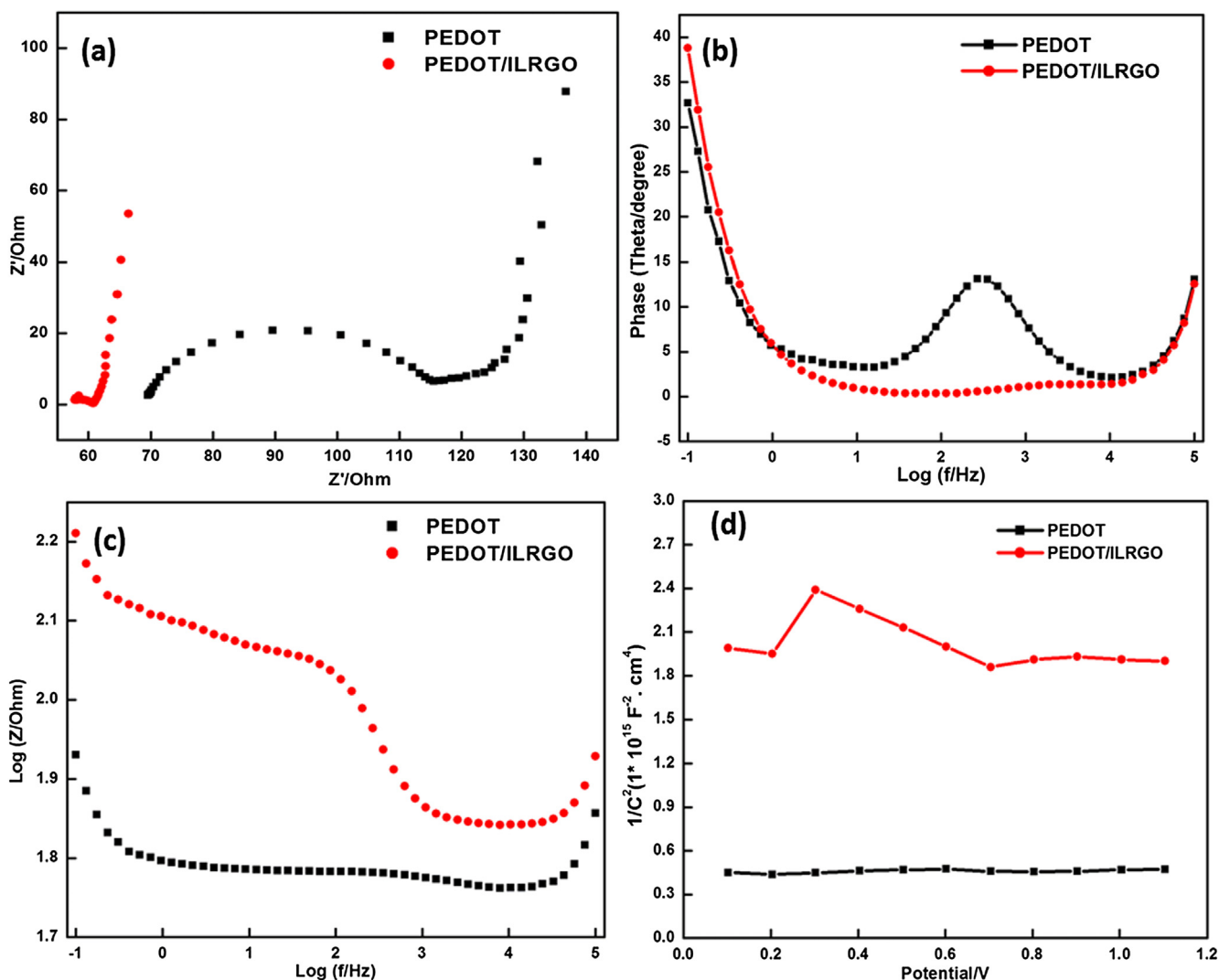


Fig. 6 (a) Nyquist plots of (■) neat PEDOT and (●) PEDOT/ILRGO in 5 mM $[\text{Fe}(\text{CN})]^{-3/-4}$ containing 0.1 M KCl in the frequency range of $0.1\text{--}10^5 \text{ Hz}$, (b) and (c) shows Bode's plots (phase angle and $\log f$, $\log Z$ vs. $\log f$) and (d) M-S plots between capacitance at varying potentials of neat PEDOT and PEDOT/ILRGO.

frequency region, it is clearly perceptible that diameter of semi-circle is decreasing in the modified electrode resulting in lesser interfacial resistance provided by higher electrical conductivity of reduced graphene oxide. The charge transfer resistance (R_{ct}) of PEDOT/ILRGO modified electrode comes out to be 3.3Ω which is also lower than neat PEDOT (45.4Ω). These results suggest the increased electron transfer rate provided by highly electroactive reduced graphene oxide due to enhanced surface concentration. The solution resistance (R_s) demonstrating the ionic conductivity of electrolytic media calculated by extrapolating $Z'' = 0$, in the higher frequency region for PEDOT/ILRGO modified electrode is 57.4Ω which is again lower than PEDOT (69.4Ω) suggesting relatively enhanced charge transfer capability owing to synergistic interactions between ILRGO and PEDOT.

The Fig. 6(b, c) shows the Bode plots of neat PEDOT and PEDOT/ILRGO modified electrode representing the variation of impedance and phase angle with frequency. The slope is lower than 1 in both cases which is indicative of pseudo-capacitive behavior provided by redox sites present in the PEDOT matrix. In middle frequency region, there is shift in phase angle from 13.4° to -0.05° after the modification of surface of PEDOT with ILRGO showing the successful grafting of ILRGO onto the PEDOT surface corroborating with FESEM findings. Also the diffused pseudo capacitance (C_D), calculated from Bode plots, for PEDOT/ILRGO comes out to be 0.019 mF/cm^2 is smaller than that of neat PEDOT (0.03 mF/cm^2) hinting at enhanced charging–discharging process owing to redox sites facilitated by the modified microstructure.

The Fig. 6(d) elucidates the Mott-Schottky (M-S) analysis for neat PEDOT and PEDOT/ILRGO modified electrodes. The neat PEDOT modified electrode shows almost flat curve pointing towards absence of charge carriers whereas PEDOT/ILRGO modified electrode exhibits a negative slope, with high charge carrier density of $0.298 \times 10^{31} \text{ carriers/cm}^3$ and flat band potential (E_{FB}) of 0.75 V , obtained by extrapolating the M-S plots to $1/C^2 = 0$. Thus, all the electrochemical

investigations clearly point to the improved electrochemical response owing to the introduction of ILRGO onto the neat PEDOT system proving it an efficient redox matrix for enzyme immobilization.

3.4. Activity of electrode towards ATChI and affinity towards enzyme

Fig. 7(a) shows the typical differential pulse voltammetry (DPV) response in absence and presence of substrate ATChI in 0.1 M PBS . The increased amperometric response of sensor in presence of substrate can be attributed to oxidation of thiocholine that is formed during the hydrolysis of ATChI by enzyme (Wei and Wang, 2015).

To determine the activity of enzyme towards prepared electrode using ATChI as substrate, Michaelis-Menten constant (K_m) was calculated using standard Lineweaver-Burk equation (Du et al., 2010a,b):

$$\frac{1}{i_s} = \left(\frac{K_m^{app}}{i_{max}} \right) \left(\frac{1}{C} \right) + \frac{1}{i_{max}} \quad (6)$$

where i_s is the current at steady state after the addition of substrate, i_{max} is the current under saturated substrate concentration and C is the concentration of substrate after additions to the bulk solution. The change in current on successive addition of different amounts of ATChI at regular intervals is revealed in Fig. 7 (b) where the graph between i_s^{-1} and C^{-1} , (inset Fig. 7(b)) is showing a linear relationship between the two.

The biosensor follows Michaelis-Menten behavior at both lower and higher concentrations with K_m value of 0.008 mM and 0.08 mM respectively, which are much lower than the reported values of 0.131 mM and 0.268 mM of SnO_2NPs -carboxylic graphene (Zhou et al., 2013) and MWCNTs-Au systems respectively (Du et al., 2010a,b). The lower K_m value suggests large electron transfer rate between layers of PEDOT/ILRGO and increased affinity for enzyme to be

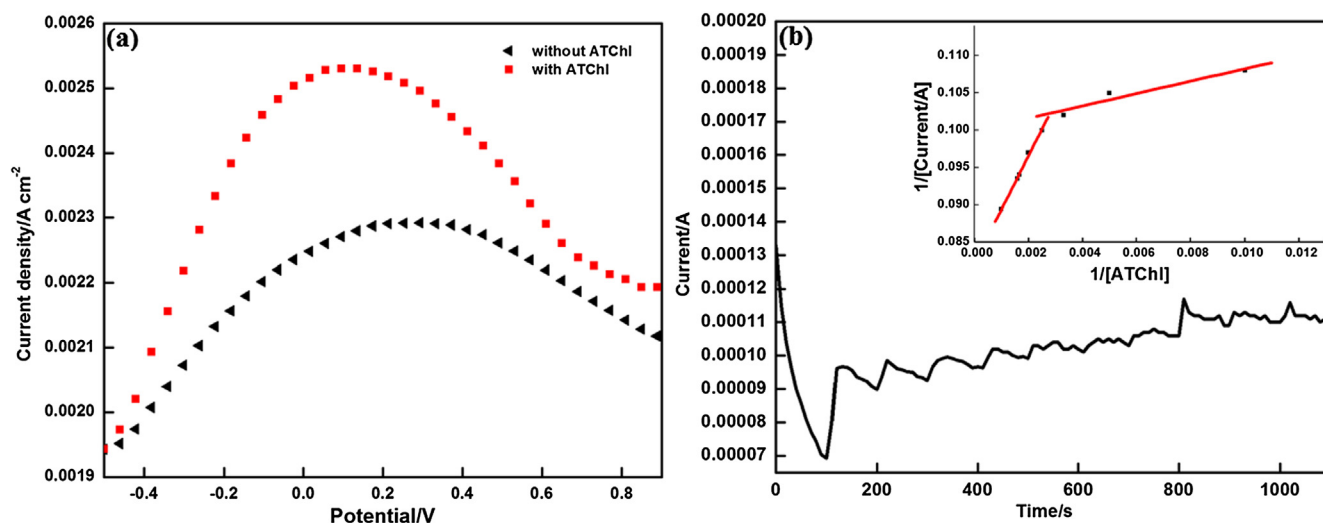


Fig. 7 (a) DPV studies of PEDOT-ILRGO/ACHE (\blacktriangle) in absence of ATChI and (\blacksquare) in presence of ATChI in 0.1 M PBS at step potential of 8 mV and 0.2 V modulation amplitude, and (b) Current-time response of sensor on addition of ATChI (in 0.1 M PBS , $\text{pH } 7.4$, 0.68 V) (Inset shows Lineweaver-Burk plot of $1/i_{ss}$ versus $1/C$).

adsorbed on the surface of electrode attributed to more hydrophilicity provided by ILRGO.

3.5. Optimization of various parameters

In order to study the inhibition mechanism and to get maximum sensitivity for increasing the performance of biosensor, we need to optimize certain parameters (Kaur et al., 2016). The pH of the medium is one such parameter which is essential to optimize considering the dependence of the activity of biomolecules on it. On recording the amperometric signal in the range of pH 6.0 to 8.0 (0.1 M PBS), the maximum peak current was recorded at pH 7.5 which was chosen for subsequent studies (Fig S5a).

The response of biosensor also depends on concentration of immobilized enzyme on the surface of prepared sensor. The lowest feasible concentration of enzyme was chosen to compromise between low enzyme loading and enough substrate signals. The results show that on changing the concentration from 0.05 mU

to 1 mU the maximum response was obtained at 25 mU (Fig. S5b). So, this concentration of enzyme was chosen for the determination of pesticides to obtain lower detection limits.

DPV response of biosensor was also checked within the linear range of 0.1 mM to 5 mM ATChI concentration to investigate the effect of substrate concentration on electrochemical response (Fig. S5c). It was observed that with increasing concentrations from 0.1 mM to 0.2 mM the peak current increases due to increased formation of thiocholine. But on further adding ATChI the peak current decreases. Therefore, 0.2 mM was taken as standard for further use.

Optimization of incubation time is also necessary to compromise between analytical time and sensitivity of biosensor. With increase in incubation time, the active sites of AChE get blocked due to which current response decreases (Fig. S5d). The current response was checked in terms of their effect on AChE activity at different incubation time (2–10 min) and the incubation time of 8 min. was selected for lower detection limits and rapid analysis.

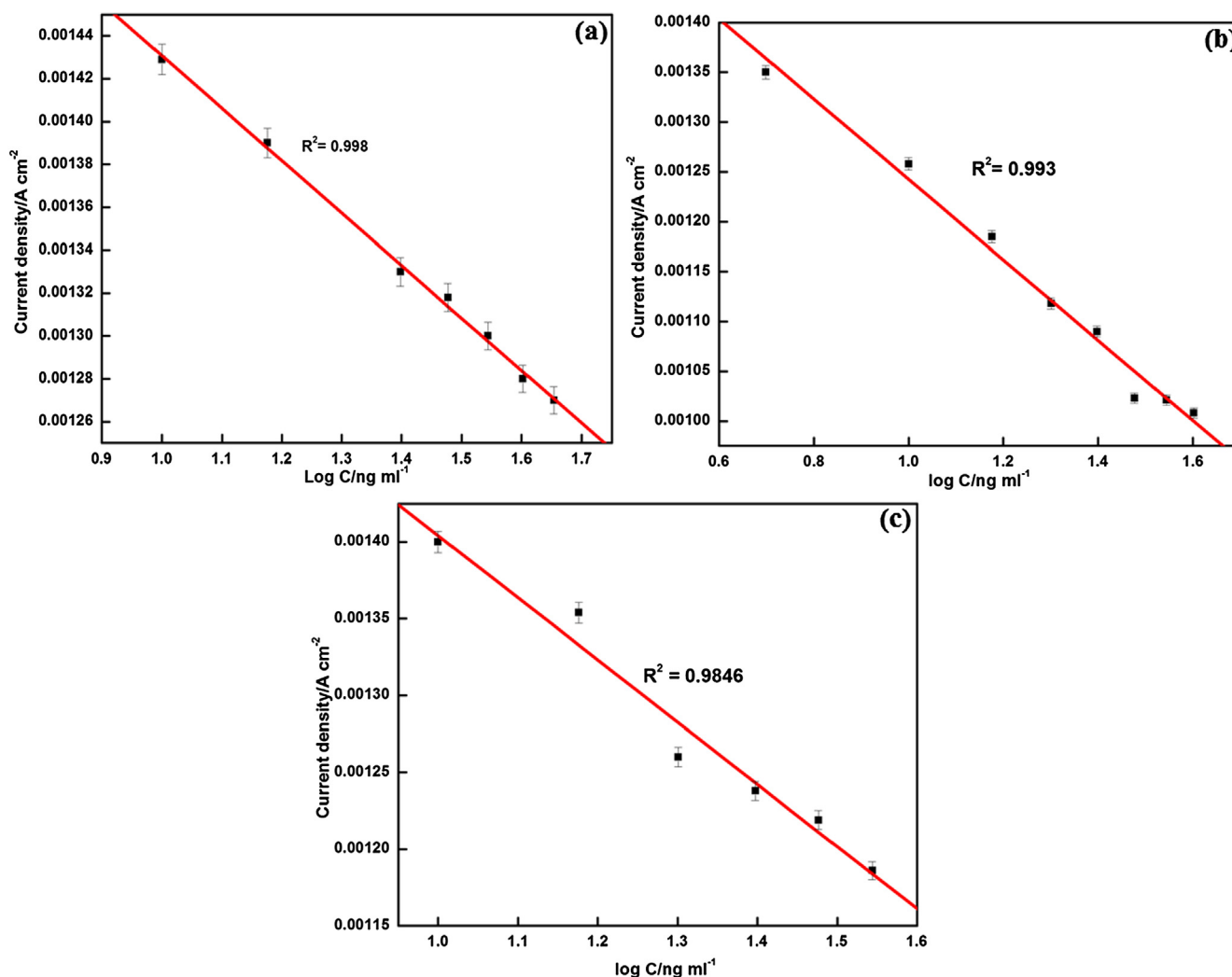


Fig. 8 Plots of current density at different concentrations of (a) chlorpyrifos (b) malathion and (c) methyl parathion in 0.1 mM PBS containing ATChI.

3.6. Pesticide detection

The designed biosensor was further utilised for the detection of OPs. After selecting the optimum incubation time, the biosensor was immersed in standard solution of three different pesticides- chlorpyrifos, malathion and methyl parathion at different concentrations and biosensor response was examined. The enzymatic biosensor works on the principle of inhibition where in the absence of analyte, ATChI gets hydrolyzed to thiocholine and acetic acid. The thiocholine thus produced undergoes oxidation at electrode on applying potential. But as OPs bind to the serine hydroxyl group of acetylcholinesterase, the resulting inhibition causes decline in the activity of enzyme (Huo et al., 2014; Chen et al., 2015; Ma and Zhang, 2011).

Henceforth, analysis should be a compromise between good detection limit and appreciable measurement period. For this, initial response of biosensor for ATChI was recorded as I_0 and then biosensor was incubated for 8 min. After rinsing the sensor with buffer solution and distilled water, the biosensing measurements were done by adding 0.2 mM ATChI into the reaction cell. The peak currents were recorded at different pesticide concentrations and it was observed that the peak current decreases with increase of pesticide concentration. The inhibition effects of different concentrations of chlorpyrifos, malathion and methyl parathion towards biosensor were investigated by studying the DPV responses before and after incuba-

tion of prepared sensor with different concentrations for 8 min. The calibration plots of all the three pesticides are shown in Fig. 8. A linear relationship was obtained for all the three pesticides with limit of detection of chlorpyrifos, malathion and methyl parathion calculated to be 0.04 ng ml^{-1} , 0.117 ng ml^{-1} and 0.108 ng ml^{-1} respectively, using 3σ method. Various parameters obtained from the calibration curve of three pesticides under optimized conditions are listed in Table S1.

This value is lower than maximum residual limit of OPs ($0.2 \mu\text{g ml}^{-1}$), hence the present method suits well for the detection of OPs in the real samples. The limit of detection of biosensor thus prepared was also better than many other nanostructure based electrochemical sensors (Table 1).

The biosensor also exhibits negligible interferences from various ions as indicated in supplementary information (Fig. S6).

3.7. Analytical applications

In order to test the validity of prepared sensor, the optimized procedure was applied for the detection of OPs in aerated dinks and apple juice samples (Figs. S7 and S8). The samples obtained were spiked with different amounts of chlorpyrifos, malathion and methylparathion. A linear plot was observed between concentration of pesticides and current density of all three pesticides. The calibration parameters and the amounts of pesticides found in various samples are listed in Table 2,

Table 1 Comparison of AChE/PEDOT/ RGO/IL/FTO biosensor with other electrochemical sensors used for the detection of OPs.

Electrode material	Pesticide	Technique	K_M value	Detection limit (ng ml^{-1})	References
PEDOT:PSS	Diethyl 4-nitrophenyl phosphate	CV	–	1.3×10^3	Hryniewicz et al. (2018)
PAnPPy-MWCNTs copolymer	Malathion	CV	–	1	Du et al. (2010a,b)
AChE-MWCNTs-Au-CHIT/GCE	Malathion	CV	$268 \mu\text{M}$	0.6	Du et al. (2010a,b)
AuNP-CS-IL/PGE	Malathion	SQV	–	0.226	Bolat and Abaci (2018)
PMG/GNs-NF/GCE	Methyl parathion	Chrono amperometry	–	0.53	Xu et al. (2012)
CNTs/CP electrode	Methyl parathion	DPV	–	3.9	Yue et al. (2016)
Biomimetic SPE/PHA/Mpeg	Chlorpyrifos	Chrono amperometry	–	0.029×10^3	Sgobbi and Machado (2018)
AChE/PEDOT/RGO/IL/FTO	Malathion	DPV	$8 \mu\text{M}$ &	0.117	This work
	Chlorpyrifos		$80 \mu\text{M}$	0.04	
	Methyl parathion			0.108	

Table 2 Various parameters obtained by using the calibration curves of real sample analysis.

Parameters	Apple Juice			Aerated drinks		
	Chlorpyrifos methyl	Malathion	Methyl parathion	Chlorpyrifos methyl	Malathion	Methyl parathion
Correlation coefficient (R)	0.984	0.982	0.978	0.9838	0.907	0.949
LOD (ng/ml)	0.169	0.183	0.202	0.176	0.44	11.68
LOQ (ng/ml)	0.564	0.613	0.667	0.58	1.48	38.96
Sensitivity	0.00154	0.00132	0.00155	0.0014	0.00144	0.00137
Amount found (ng/ml)	1.03	1.36	2.74	4.2	2.26	6.64

representing that it is less than the permissible level in real food samples.

3.8. Reactivation and storage stability

The biosensor was stored at 4 °C when not in use to check the storage stability of prepared electrode system. The storage stability of biosensor was checked after some days. The biosensor retained its 100% current response after 7 days and almost negligible peak potential shift was seen. The response was again checked after 15 days of storage stability. The sensor retained 95.7% of initial current response after 15 days. Thus, the biosensor has appreciable stability upto 15 days.

The regeneration of biosensor was checked by immersing it in chlorpyrifos, malathion, methyl-parathion solution for 8 min. and then transferred into 2-pyridinealdoxime methiodide (2-PAM) (10 mM solution) for different time periods and current response was checked. It was observed that sensor could regain 91.7% of its initial activity after incubation with 2-PAM for 8 min.

4. Conclusions

An efficient electrochemical sensor based on active enzyme (AChE) using PEDOT/ILRGO as immobilization matrix was developed for quantification of OPs by employing a simple methodology. The modification of reduced graphene oxide with imidazolium based ionic liquid has resulted in well interspersed RGO structures onto the PEDOT matrix owing to the increased hydrophilicity. The superiority of this ionic liquid functionalization approach is that it has fortified the designed electrode with larger number of redox sites resulting in higher electron transfer rate thereby boosting its electrocatalytic activity with prevention of the electrode fouling. The designed microstructure has enabled the sensor to show high affinity towards substrate with apparent Michaelis constant 0.008 mM and 0.08 mM at lower and higher concentrations respectively. The electrochemical analysis clearly demonstrates the effect of better enzyme loading and higher current response in the proposed sensor. The proposed method offers long term storage stability with successful reactivation with 2-PAM along with efficient infield analysis of the real samples. High sensitivity and selectivity even in case of real samples for all the three organophosphorus pesticides with good reproducibility has made the designed biosensor an apt candidate in the field of organophosphorus pesticide's detection.

Acknowledgements

Financial grant from Department of Science and Technology-Science and Engineering Research Board (Grant No. SERB/F/0635) is gratefully acknowledged by the authors. Authors are thankful to Dr. Suman Singh, Senior scientist, CSIO for contact angle measurements.

Appendix A. Supplementary material

Supplementary data associated with this article can be found, in the online version, at <https://doi.org/10.1016/j.arabjc.2018.08.008>.

References

- Ahmed, R., Reifsnider, K., 2011. Study of influence of electrode geometry on impedance spectroscopy. *Int. J. Electrochem. Sci.* 6, 1159–1174.
- Bahadır, E.B., Sezginürk, M.K., 2016. Applications of graphene in electrochemical sensing and biosensing. *Trend Anal. Chem.* 76, 1–14.
- Bhadekar, R., Pote, S., Tale, V., Nirichan, B., 2011. Developments in analytical methods for detection of pesticides in environmental samples. *Am. J. Analyt. Chem.* 2, 1–15.
- Bhandari, S., Deepa, M., Srivastava, A.K., 2009. Poly(3,4-ethylenedioxythiophene)-multiwalled carbon nanotube composite films: Structure-directed amplified electrochromic response and improved redox activity. *J. Phys. Chem. B* 113, 9416–9428.
- Bolat, G., Abaci, S., 2018. Non-enzymatic electrochemical sensing of malathion pesticide in tomato and apple samples based on gold nanoparticles-chitosan-ionic liquid hybrid nanocomposite. *Sensors* 18, 773–789.
- Chen, D., Jiao, Y., Jia, H., Guo, Y., Sun, X., Wang, X., Xu, J., 2015. Acetylcholinesterase biosensor for chlorpyrifos detection based on multi-walled carbon nanotubes-SnO₂-chitosan nanocomposite modified screen-printed electrode. *Int. J. Electrochem. Sci.* 10, 10491–10501.
- Chowdhary, S., Bhattacharyya, R., Banerjee, D., 2014. Acute organophosphorus poisoning. *Clin. Chim. Acta* 431, 66–76.
- De Silva, K.S.B., Gambhir, S., Wang, X.L., Xu, X., Li, W.X., Officer, D.L., Wexler, D., Wallace, G.G., Dou, S.X., 2012. The effect of reduced graphene oxide addition on the superconductivity of MgB₂. *J. Mater. Chem.* 22, 13941–13946.
- Du, D., Wang, M., Cai, J., Qin, Y., Zhang, A., 2010a. One-step synthesis of multiwalled carbon nanotubes-gold nanocomposites for fabricating amperometric acetylcholinesterase biosensor. *Sens. Actuat. B* 143, 524–529.
- Du, D., Ye, X., Cai, J., Liu, J., Zhang, A., 2010b. Acetylcholinesterase biosensor design based on carbon nanotube-encapsulated polypyrrole and polyaniline copolymer for amperometric detection of organophosphates. *Biosens. Bioelectron.* 25, 2503–2508.
- Farghaly, O.A., Abdel Hameed, R.S., Abou-Nawwas, A.H., 2014. Analytical application using modern electrochemical techniques. *Int. J. Electrochem. Sci.* 9, 3287–3318.
- Fragkou, V., Ge, Y., Steiner, G., Freeman, D., Bartetzko, N., Turner, A.P.F., 2012. Determination of the real surface area of a screen-printed electrode by chronocoulometry. *Int. J. Electrochem. Sci.* 7, 6214–6220.
- Harshit, D., Charmy, K., Nrupesh, P., 2017. Organophosphorus pesticides determination by novel HPLC and spectrophotometric method. *Food Chem.* 230, 448–453.
- Hryniewicz, B.M., Orth, E.S., Viddoti, M., 2018. Enzymeless PEDOT-based electrochemical sensor for the detection of nitrophenols and organophosphates. *Sens. Actuat. B* 257, 570–578.
- Huang, T., Kung, C., Wang, J., Lee, M., Chen, L., Chu, C., Ho, K., 2015. Graphene nanosheets/poly(3,4-ethylenedioxythiophene) nanotubes composite materials for electrochemical biosensing applications. *Electrochim. Acta* 172, 61–70.
- Huang, Y., Li, H., Balogun, M., Liu, W., Tong, Y., Lu, X., Ji, H., 2014. Oxygen vacancy induced bismuth oxyiodide with remarkably increased visible-light adsorption and superior photocatalytic performance. *ACS Appl. Mater. Interfaces* 6, 22920–22927.
- Huang, Y., Xu, H., Yang, H., Lin, Y., Liu, H., Tong, Y., 2018b. Efficient charges separation using advanced BiOI-based hollow spheres decorated with palladium and manganese dioxide nanoparticles. *ACS Sustain. Chem. Eng.* 6, 2751–2757.
- Huang, Y., Li, K., Lin, Y., Tong, Y., Liu, H., 2018c. Enhanced efficiency of electron-hole separation in Bi₂O₂CO₃ for photocatalysis via acid treatment. *Chem. Cat. Chem.* 10, 1982–1987.

- Huang, Y., Lee, H.K., Shih, K., Jen, J., 2018a. A sublimate sorbent for stir-bar sorptive extraction of aqueous endocrine disruptor pesticides for gas-chromatography-electron capture detection. *J. Chromatogr. A* 1564, 51–58.
- Huo, D., Li, Q., Zhang, Y., Houa, C., Lei, Y., 2014. A highly efficient organophosphorus pesticides sensor based on CuO nanowires–SWCNTs hybrid nanocomposite. *Sens. Actuat. B* 199, 410–417.
- Ji, Z., Zhu, G., Shen, X., Zhou, H., Wu, C., Wang, M., 2012. Reduced graphene oxide supported Fe-Pt alloy nanoparticles with high electrocatalytic performance for methanol oxidation. *New J. Chem.* 36, 1774–1780.
- Karthik, P., Vinoth, R., Zhang, P., Choi, W., Balaraman, E., Neppolian, B., 2018. II- II interaction between metal-organic framework and reduced graphene oxide for visible-light photocatalytic H₂ production. *ACS Appl. Energy Mater.* 1, 1913–1923.
- Kaur, N., Thakur, H., Prabhakar, N., 2016. Conducting polymer and multi-walled carbon nanotubes nanocomposites based amperometric biosensor for detection of organophosphate. *J. Electroanal. Chem.* 775, 121–128.
- Kumar, P., Kim, K., Deep, A., 2015. Recent advancements in sensing techniques based on functional materials for organophosphate pesticides. *Biosens. Bioelectron.* 70, 469–489.
- Lee, M., Balasingam, S.K., Jeong, H.Y., Hong, W.G., Lee, H., Kim, B.H., Jun, Y., 2015. One-step hydrothermal synthesis of graphene decorated V₂O₅ nanobelts for enhanced electrochemical energy storage. *Sci. Rep.* 5, 8151. <https://doi.org/10.1038/srep08151>.
- Liu, Q., Fei, A., Huan, J., Mao, H., Wang, K., 2015. Effective amperometric biosensor for carbaryl detection based on covalent immobilization acetylcholinesterase on multiwall carbon nanotubes/graphene oxide nanoribbons nanostructure. *J. Electroanal. Chem.* 740, 8–13.
- Liu, G., Li, L., Huang, X., Zheng, S., Xu, D., Xu, X., Zhang, Y., Lin, H., 2018. Determination of triazole pesticides in aqueous solution based on magnetic graphene oxide functionalized MOF-199 as solid phase extraction sorbents. *Microporous Mesoporous Mater.* 270, 258–264.
- Liu, L., Suryoprabowo, S., Zheng, Q., Song, S., Kuang, H., 2017. Rapid detection of aldicarb in cucumber with an immunochromatographic test strip. *Food Agr. Immunol.* 28, 427–438.
- Lv, S., Zhang, K., Zeng, Y., Tang, D., 2018. Double photosystems-based 'Z-Scheme' photoelectrochemical sensing mode for ultrasensitive detection of disease biomarker accompanying three dimensional DNA walker. *Anal. Chem.* 90, 7086–7093.
- Ma, J., Zhang, W., 2011. Gold nanoparticle-coated multiwall carbon nanotube-modified electrode for electrochemical determination of methyl parathion. *Microchim. Acta* 175, 309–314.
- Moyo, M., Okonkwo, J.O., Agyei, N.M., 2012. Recent advances in polymeric materials used as electron mediators and immobilizing matrices in developing enzyme electrodes. *Sensors* 12, 923–953.
- Muthosamy, K., Bai, R.G., Abubakar, I.B., Sudheer, S.M., Lim, H. N., Loh, H., Huang, N.M., Chia, C.H., Manickam, S., 2015. Exceedingly biocompatible and thin-layered reduced graphene oxide nanosheets using an eco-friendly mushroom extract strategy. *Int. J. Nanomed.* 10, 1505–1519.
- Narayana, P.V., Reddy, T.M., Gopal, P., Raghu, P., Reddaiah, K., Srinivasulu, M., 2014. Development of trypan blue polymer film based electrochemical sensor for the determination of dopamine and its simultaneous detection in presence of ascorbic acid and uric acid: a voltammetric method. *Anal. Bioanal. Electrochem.* 6, 485–500.
- Obare, S.O., De, C., Guo, W., Haywood, T.L., Samuels, T.A., Adams, C.P., Masika, N.O., Murray, D.H., Anderson, G.A., Campbell, K., Fletcher, K., 2010. Fluorescent chemosensors for toxic organophosphorus pesticides: a review. *Sensors* 10, 7018–7043.
- Pundir, C.S., Chauhan, N., 2012. Acetylcholinesterase inhibition-based biosensors for pesticide determination: a review. *Anal. Biochem.* 429, 19–31.
- Qiu, Z., Shu, J., Tang, D., 2018. Near-infrared-to-ultraviolet light-mediated photochemical aptasensing platform for cancer biomarker based on core shell NaYF₄:Yb, Tm@TiO₂ upconversion microrods. *Anal. Chem.* 90, 1021–1028.
- Saxena, A.P., Deepa, M., Joshi, A.G., Bhandari, S., Srivastava, A.K., 2010. Poly(3,4-ethylenedioxythiophene)-ionic liquid functionalized graphene/reduced graphene oxide nanostructures: Improved conduction and electrochromism. *ACS Appl. Mater. Interfaces* 3, 1115–1126.
- Sgobbi, L.F., Machado, S.A.S., 2018. Functionalized polyacrylamide as an acetylcholinesterase-inspired biomimetic device for electrochemical sensing of organophosphorus pesticides. *Biosens. Bioelectron.* 100, 290–297.
- Shahriary, L., Athawale, A.A., 2014. Graphene oxide synthesized by using modified hummers approach. *Int. J. renew. Energy environ. Eng.* 2, 58–63.
- Shen, F., Wang, Y., Li, S., Liu, J., Dong, L., Wei, T., Wu, X., Lan, Y., 2013. Self-assembly of polyoxometalate/ Reduced graphene oxide composites induced by ionic liquids as high rate cathode for batteries: Killing two birds with one stone. *J. Mater. Chem. A* 6, 1743–1750.
- Shu, J., Qiu, Z., Lv, S., Zhang, K., Tang, D., 2018. Plasmonic enhancement coupling with defect-engineered TiO_{2-x}: a mode for sensitive photoelectrochemical biosensing. *Anal. Chem.* 90, 2425–2429.
- Shu, J., Tang, D., 2017. Current advances in quantum-dots-based photoelectrochemical immunoassays. *Chem. Asian J.* 12, 2780–2789.
- Sikora, T., Istamboulie, G., Jubete, E., Ochoteco, E., Marty, J., Noguez, T., 2011. Highly Sensitive Detection of organophosphate insecticides using biosensors based on genetically engineered acetylcholinesterase and poly(3,4-ethylenedioxythiophene). *J. Sensors* 2011, 1–7.
- Soltani, T., Lee, B., 2017. A benign ultrasonic route to reduced graphene oxide from pristine graphite. *J. Colloid Interface Sci.* 486, 337–343.
- Sundramoorthy, A.K., Premkumar, B.S., Gunasekaran, S., 2016. Reduced graphene oxide-poly(3,4-ethylenedioxythiophene)-polystyrenesulfonate based dual-selective sensor for iron in different oxidation states. *ACS Sens.* 1, 151–157.
- Tang, D., Yuan, R., Chai, Y., 2006. Ligand functionalized core/shell Ag@Au nanoparticles Label-free amperometric immunobiosensor. *Biotechnol. Bioeng.* 94, 996–1004.
- Taylor, I.M., Robbins, E.M., Catt, K.A., Cody, P.A., Happe, C.L., Cui, X.T., 2017. Enhanced dopamine detection sensitivity by PEDOT/graphene oxide coating on in vivo carbon fibre electrodes. *Biosens. Bioelectron.* 89, 400–410.
- Wang, G., Tan, X., Zhou, Q., Liu, Y., Wang, M., Yang, L., 2014. Synthesis of highly dispersed zinc oxide nanoparticles on carboxylic graphene for development a sensitive acetylcholinesterase biosensor. *Sens. Actuat. B* 190, 730–736.
- Wei, M., Wang, J., 2015. A novel acetylcholinesterase biosensor based on ionic liquids-AuNPs-porous carbon composite matrix for detection of organophosphate pesticides. *Sens. Actuat. B* 211, 290–296.
- Wu, L., Lei, W., Han, Z., Zhang, Y., Xia, M., Hao, Q., 2015. A novel non-enzyme amperometric platform based on poly(3-methylthiophene)/nitrogen doped graphene modified electrode for determination of trace amounts of pesticide phoxim. *Sens. Actuat. B* 206, 495–501.
- Wu, N., She, X., Yang, D., Wu, X., Su, F., Chen, Y., 2012. Synthesis of network reduced graphene oxide in polystyrene matrix by a two-step reduction method for superior conductivity of the composite. *J. Mater. Chem.* 22, 17254–17261.
- Xie, Z., Kong, D., Liu, L., Song, S., Kuang, H., 2017. Development of ic-ELSA and lateral flow immunochromatographic assay strip for the simultaneous detection of avermectin and ivermectin. *Food Agr. Immunol.* 28, 439–451.

- Xu, M., Zhu, J., Su, H., Dong, J., Ai, S., Li, R., 2012. Electrochemical determination of methyl parathion using poly(malachite green)/graphene nanosheets–nafion composite film-modified glassy carbon electrode. *J. Appl. Electrochem.* 42, 509–516.
- Yao, L., Liu, L., Song, S., Kuang, H., Xu, C., 2017. Development of indirect competitive enzyme-linked immunosorbent and immunochromatographic strip assays for carbofuran detection in fruits and vegetables. *Food Agr. Immunol.* 28, 639–651.
- Yue, X., Han, P., Zhu, W., Wang, J., Zhang, L., 2016. Facile and sensitive electrochemical detection of methyl parathion based on a sensing platform constructed by the direct growth of carbon nanotubes on carbon paper. *RSC Adv.* 6, 58771–58805.
- Zheng, Y., Liu, Z., Jing, Y., Lie, J., Zhan, H., 2015. An acetylcholinesterase biosensor based on ionic liquid functionalized graphene-gelatin-modified electrode for sensitive detection of pesticides. *Sens. Actuat. B* 210, 389–397.
- Zhou, Q., Yang, L., Wang, G., Yang, Y., 2013. Acetylcholinesterase biosensor based on SnO₂nanoparticles–carboxylic graphene–nafion modified electrode for detection of pesticides. *Biosens. Bioelectron.* 49, 25–31.